Recent unprecedented change of Pacific decadal variability shows a fingerprint of anthropogenic forcing

Weiyi Sun[1], Bin Wang[2], Jian Liu[3], and Yifei Dai[4]

[1]Key Laboratory for Virtual Geographic Environment, Ministry of Education; State Key Laboratory Cultivation Base of Geographical Environment Evolution of Jiangsu Province; Jiangsu Center for Collaborative Innovation in Geographical Information Resource Development and ApplicationSchool of Geography Science, Nanjing Normal University, Nanjing 210023, China
[2]Department of Atmospheric Sciences and International Pacific Research Center,University of Hawaii
[3]Nanjing Normal University
[4]Nanjing University of Information Science and Technology

November 23, 2022

Abstract

How the Pacific Decadal Variability (PDV) would change under a warming world remains an issue of scientific debate and societal concern. Here we show that the PDV has been experiencing an unprecedented change in the last two decades. The PDV has amplified along the west coast of North America and equatorial central Pacific while weakened over the South Pacific and Kuroshio-Oyashio Extension (KOE) region. Examination of 33 CMIP6 models' ensemble mean projection reveals that anthropogenic radiative forcing may weaken the PDV variability in the South Pacific and KOE region, suggesting part of the observed change may be attributed to anthropogenic forcing. However, the recently increased decadal variability over the western North American coast and equatorial central Pacific may be part of the internal variability arising from increased coupling between the positive Pacific Decadal Oscillation (PDO) and negative North Pacific Gyre Oscillation (NPGO).

Recent unprecedented change of Pacific decadal variability shows a fingerprint of anthropogenic forcing

Weiyi Sun[1], Bin Wang[2,3], Jian Liu[1,4,5*], and Yifei Dai[3]

[1]Key Laboratory for Virtual Geographic Environment, Ministry of Education; State Key Laboratory Cultivation Base of Geographical Environment Evolution of Jiangsu Province; Jiangsu Center for Collaborative Innovation in Geographical Information Resource Development and Application; School of Geography Science, Nanjing Normal University, Nanjing 210023, China

[2]Department of Atmospheric Sciences and Atmosphere-Ocean Research Center, University of Hawaii at Manoa, Honolulu, HI 96825, USA

[3]Key Laboratory of Meteorological Disaster of Ministry of Education and Earth System Modeling Center, Nanjing University of Information Science and Technology, Nanjing 210044, China

[4]Jiangsu Provincial Key Laboratory for Numerical Simulation of Large Scale Complex Systems, School of Mathematical Science, Nanjing Normal University, Nanjing 210023, China

[5]Open Studio for the Simulation of Ocean-Climate-Isotope, Qingdao National Laboratory for Marine Science and Technology, Qingdao 266237, China

Corresponding author: Jian Liu (jliu@njnu.edu.cn)

Key Points:

- PDV has experienced an unprecedented change during the last two decades.
- Anthropogenic forcing may play a role in weakening the PDV in the South Pacific and KOE region.
- The increased variability over the western North American coast and equatorial central Pacific may be part of the internal variability.

Abstract

How the Pacific Decadal Variability (PDV) would change under a warming world remains an issue of scientific debate and societal concern. Here we show that the PDV has been experiencing an unprecedented change in the last two decades. The PDV has amplified along the west coast of North America and equatorial central Pacific while weakened over the South Pacific and Kuroshio-Oyashio Extension (KOE) region. Examination of 33 CMIP6 models' ensemble mean projection reveals that anthropogenic radiative forcing may weaken the PDV variability in the South Pacific and KOE region, suggesting part of the observed change may be attributed to anthropogenic forcing. However, the recently increased decadal variability over the western North American coast and equatorial central Pacific may be part of the internal variability arising from increased coupling between the positive Pacific Decadal Oscillation (PDO) and negative North Pacific Gyre Oscillation (NPGO).

Plain Language Summary

Pacific Decadal Variability (PDV) is one of the primary modes of internal variability. There is an unprecedented change of the PDV after 1999, which has remarkably altered its impacts on global atmospheric circulation and land precipitation. The amplitude of PDV has decreased over the South Pacific and Kuroshio-Oyashio Extension (KOE) region but strengthened along the west coast of North America and equatorial central Pacific. The recent change in PDV can be induced by a combination of the internal climate variability and anthropogenic warming. The 33 CMIP6 models' ensemble mean projects that future anthropogenic warming will weaken the PDV variability in most regions of the Pacific, especially in the KOE region and South Pacific. However, the recent increased PDV amplitude over the west coast of North American and equatorial central Pacific may be due to the increased coupling between the Pacific Decadal Oscillation and North Pacific Gyre Oscillation.

1 Introduction

Pacific Decadal Variability (PDV) has profound impacts on the North Pacific ecosystems and socio-economical fisheries and influences climate variation and predictability in Eurasia and North America (Liu & Di Lorenzo, 2018; Liguori & Di Lorenzo, 2018; Dai, 2013; Liu, 2012; Whitney, 2014). The term PDV used here refers to the Pacific Decadal Oscillation (PDO), Interdecadal Pacific Oscillation (IPO), and South Pacific Decadal Oscillation (SPDO) (Mantua et al., 1997; Schneider et al., 2002; Kwon & Deser, 2007; Mo, 2000; Power et al., 1999; Chen & Wallace, 2015). Although IPO is defined in different domains, and the corresponding patterns are not identical to PDO, its temporal variation is highly correlated with PDO/SPDO. Many studies analyzed the impacts of PDO/IPO on global land precipitation before 2013 (Newman et al., 2016; Lyon et al., 2014; Qin et al., 2018), but few studies examine the recent change of the PDV pattern and its impacts in the past two decades.

Unprecedented warming occurred over the Northeastern Pacific from 2014 through 2016, which induced the largest marine heatwave ever recorded (Di Lorenzo & Mantua, 2016). Some studies explained that the change of atmospheric variability influenced the Northeastern Pacific warming during the winter of 2013/14, which might have a tropical origin (Wang et al., 2015; Hartmann, 2015; Seager et al., 2015). The persistence of the Northeastern Pacific warming is found to be related to a warm phase of North Pacific Gyre Oscillation (NPGO) and PDO (Di Lorenzo & Mantua, 2016; Di Lorenzo et al., 2008). Further, a significant correlation (R=0.6) between the negative winter NPGO and the following winter PDO is found during 1985-2015, which induces more multi-year warm SST events over the Northeast Pacific (Joh & Di Lorenzo, 2017). Note that these investigations focus on the interannual time scale, and our knowledge of the changes in decadal variability remains a gap.

Over the past two decades, global ocean heat content experienced an acceleration of warming, with the most massive warming in the tropical/subtropical Pacific Ocean and the southern oceans (Cheng et al., 2017). It is curious whether the most extensive oceanic warming may change the PDV or the other way around. To this end, an examination of the projected future changes of PDO under anthropogenic warming would be useful. The Fifth Assessment Report (AR5) concluded that near-term predictions of PDV were largely model dependent (Van Oldenborgh et al., 2012), and the projections made by the state-of-the-art coupled general circulation models had yielded inconsistent results. Some projected that the variances of PDO and tropical PDV would increase in a warmer climate by using the Community Earth System Model Large Ensemble (Lorenzo & Mantua, 2016; Liguori & Di Lorenzo, 2018). On the other hand, some CMIP5 models' projections suggested the suppressed PDO variability and shortened periodicity (Zhang & Delworth, 2016; Geng et al., 2019; Li et al., 2020).To our knowledge, no study draws attention on the change of the decadal variability over the South Pacific in future warming, although it is an essential part of PDV.

2 Methods

2.1 Observational and modeling data

The ensemble mean of two sets of SST data is used in this study. One is the Extended Reconstructed Sea Surface Temperature, version 5 (ERSST v5) global SST monthly data on a 2° × 2° horizontal grid from January 1854 to the present (Huang et al., 2017). Another is the Hadley

Center Sea Ice and SST dataset version 1.1 (HadISST 1.1) with a 1 ° × 1 °resolution from 1871 to the present (Rayner et al., 2003). For precipitation, we used the Global Precipitation Climatology Center (GPCC) dataset overland on a 1 °×1 ° grid (Schneider et al., 2014). The atmospheric circulation fields are derived from the European Center for Medium-Range Weather Forecasts (ECMWF) reanalysis dataset by merging the ERA 40-year reanalysis (ERA-40) during the period 1958-2001 (Uppala et al., 2005) and the ERA-5 reanalysis during the period 1979-2019 (Hersbach et al., 2018). To ensure the data consistency, we combine the ERA-40 and the ERA-5 data by calibrating the ERA-40 based on the monthly climatology of the ERA-5 during the overlap period (1979-2001). We focus on the decadal phase change over the Pacific from 1958-2019 because the reanalysis data (ERA-40) begin in 1958. All variables are detrended during this period.

To investigate the influence of global warming on PDV, we examined 33 CMIP6 coupled global climate models forced by the historical natural and anthropogenic forcings and by the future greenhouse gases under the Shared Socioeconomic Pathway 5-8.5 (SSP5-8.5) scenario (Eyring et al., 2016). The temporal coverage is from 1905-2005 in the historical simulations, and 2020-2100 in the SSP5-8.5 runs. Meanwhile, we also use the historical and representative concentration pathway 8.5 (RCP8.5) scenarios from 36 CMIP5 models for comparison (Taylor et al., 2012). The observational and models' data are aggregated to a grid resolution of 2.5 °latitude by 2.5 °longitude using bilinear interpolation.

2.2 The first baroclinic oceanic Rossby wave speed

The SST decadal variability is associated with the adjustment of ocean gyre circulation through the westward propagating Rossby waves (Schneider et al., 2002; Kwon & Deser, 2007; Newman et al., 2016). In a warmer climate, the phase speed of the first-baroclinic oceanic Rossby wave is projected to increase over the North Pacific, which alters the time scale and amplitude of the PDO (Zhang & Delworth, 2016; Geng et al., 2019; Li et al., 2020). In this study, we examine the first baroclinic Rossby wave speed over the entire Pacific (outside of the equatorial band) under the historical and greenhouse warming scenarios from CMIP6 models. Following the method proposed by Chelton et al. (1998), the *n*-mode Rossby radius of deformation can be defined by

$$\lambda_n = \frac{1}{n\pi|f|}\int_{-H}^{0} N(z)\,dz\,, \qquad n \geq 1, \tag{1}$$

where $f = 2\Omega sin\vartheta$ represents the Coriolis parameter for latitude ϑ and earth rotation rate Ω, H is the depth of the local water, and $N(z)$ denotes the buoyancy frequency, which can be further expressed as

$$N^2(z) = -\frac{g}{\rho}\frac{\partial\rho}{\partial z} - \frac{g^2}{c_s^2}\,, \tag{2}$$

where ρ is the water density, c_s is the sound speed. The first baroclinic oceanic Rossby wave speed ($C_1 = -\beta\lambda_1^2$) can be written as

$$C_1 = -\beta\left[\frac{1}{\pi|f|}\int_{-H}^{0} N(z)dz\right]^2 \tag{3}$$

where β denotes the meridional gradient of the Coriolis parameter f.

3 Remarkable change in PDV toward the end of the 20th century

Previous studies showed that the definition of PDV is the leading EOF mode of low-pass filtered SST anomalies (SSTA) over the Pacific basin (45 °S-65 °N) (Liu & Di Lorenzo, 2018), but some studies also found the South Pacific decadal variability could extend to about 60 °S (Hus & Chen, 2011; Zhang et al., 2018). To describe the decadal variability over the entire Pacific, we depict the PDV using the first EOF mode of SSTA over the entire Pacific basin (70 °S-70 °N) and define the PDV index using the time series of the first principal component. We used the 30-month running mean data to obtain the PDV index (Fig 1a). The PDV index is similar to the PDO index derived by using the data north of the 20 °N with a correlation coefficient of 0.86 between them during 1901-2019 ($p<0.01$). After 1958, the PDV index shows two cold (negative) phases (1961-1976 (D1) and 1999-2013 (D3)), and two warm (positive) phases (1977-1998 (D2) and 2014-2019 (D4)). The last warm phase might not have completed yet. These positive and negative phases are also the same as the PDO, indicating that the PDV index represents very well the Pacific basin-wide decadal variability.

To detect the recent change in the spatial pattern of PDV, we compare the differences in the anomalous annual mean SST between (D2 minus D1) and (D4 minus D3). During the first PDV cycle from 1961 to 1998, the warm-minus-cold phase (D2-D1) features an equatorially symmetric SST anomaly pattern with a warming in the eastern Pacific triangle region surrounded by a K-shape cooling region in the western Pacific between 40 °S and 40 °N (Fig. 1b). In contrast, during the recent period (1999-2019), the warm-minus-cold phase (D4-D3) features a highly asymmetric pattern between the North and South Pacific (Fig. 1c). The cooling over the Kuroshio-Oyashio extension (KOE) region is much weaker; meanwhile, the warming along the west coast of North America and the equatorial central Pacific is much stronger than those for the D2-D1 (Fig. 1d). The magnitude of decadal change in the South Pacific is considerably weaker for the D4-D3, especially the cooling in the western South Pacific and the warming in the South Pacific cold tongue, the west coast of South America, and the southern Pacific Ocean along 60 °S (Fig. 1d).

The recent change of PDV after 1999 is unprecedented over the past 120 years, which is evidenced by an examination of the change of the leading EOF mode of the Pacific SST. The composite warm-minus-cold phase of PDV during 1961-1998 (Fig. 1b) bears a close similarity to the leading EOF mode of Pacific SSTA during the same period (Fig. S1e). Likewise, the D4-D3 of the PDV during 1999-2019 (Fig. 1c) is very similar to the leading EOF mode of Pacific SSTA during the same period (Fig. S1g). This suggests that the leading EOF mode has changed around 1998 from the equatorial symmetric pattern to the asymmetric pattern. The leading EOF mode has little change from 1901-1960 to 1961-1997 (Figs. S1c and e), suggesting that the notable recent change of PDV after 1999 is unique over the past 120 years. Note that the amplitude of South Pacific SSTA decreases drastically during D3 and D4 in comparison with those during D1 and D2 (Fig. S2).

The change of PDV is associated with changes in the atmospheric circulation and atmosphere-ocean interaction. In D2-D1, the abnormal low sea level pressure (SLP) occurs over the North and South Pacific (Fig. 1e), inducing the cyclonic anomalies, forming the symmetric dipole SST patterns (Fig. 1b), which in turn enhance the atmospheric circulation (Liu, 2012; Newman et al., 2016). However, in D4-D3, the anomalous North Pacific low SLP and associated atmosphere-ocean feedback shifted southeastward (Fig. 1f). Over the eastern South Pacific, the anomalous low SLP disappears, significantly weakening the open ocean and coastal warming.

The PDV pattern changes exert notable impacts on global land precipitation (Fig. 2a and b). Precipitation anomalies reverse their signs between D2-D1 and D4-D3 over high-latitudes (north of 50 °N) of North America and Greenland, Siberia, and western Europe, as well as tropical Africa. During the recent PDV warm phase (D4-D3), the mid-latitude East Asia and North America become significantly wetter, while Southern Africa, Northern Australia, and northeastern South America become significantly drier (Fig. 2b). Over the ocean, we have to examine the vertical motion field due to a lack of reliable precipitation observation. From the 1958-1998 cycle to 1999-2019, the anomalous vertical motion pattern in the North Pacific tends to move southeastward to the eastern North Pacific, and a substantial descending motion occurs over the tropical western Pacific (Fig. 2 c and d). The large descending motion occurs over northeastern South America is consistent with the suppressed local precipitation, which may increase the tropical African precipitation by enhancing westerlies over the tropical Atlantic (Fig. 2b). In most land areas of the world, the PDV's impact on precipitation has been changed since the D3 (Fig. S2). Overall, the D4-D3 has a stronger impact and different pattern on global land precipitation compared to those in D2-D1, which means that the teleconnection derived from the 20th century's PDV that is used for the prediction of decadal variations of the land precipitation is no longer applicable at the current cycle in the 21st century.

4 Causes of the recent PDV change

What caused the PDV change with the reduced variability in the northwestern and South Pacific and the enhanced variability in the eastern North Pacific and equatorial central Pacific? Our general hypothesis is that the PDV change is induced by a combination of anthropogenic warming and internal climate variability.

To investigate the possible anthropogenic warming's influence of the PDV, we examine the results from 33 CMIP6 historical and SSP5-8.5 scenarios (see Methods). The linear trend at each grid point is removed and the SST is processed by a 7-yr low-pass filter. The multi-model ensemble mean (MME) of the first EOF mode shows that the amplitude of the PDV pattern is suppressed in the SSP5-8.5 (Fig. 3a and b). A negative PDV pattern occurs in the difference between SSP5-8.5 and historical scenarios (Fig. 3c). Over the North Pacific, a weakened decadal variability over the KOE and western North American coast imply a decreased PDO-like pattern similar to the previous results obtained from the CMIP5 models (Geng et al., 2019; Li et al., 2020). Notably, the PDV over the South Pacific is more reduced compared to the North Pacific. To confirm this, we investigated the changes in the standard deviation (STD) of the decadal SST variability over the entire Pacific under a warming climate derived from both the CMIP5 and CMIP6 models (Fig. S3). Both CMIP5 and CMIP6 models projected a general reduction of the PDV variability, especially over the KOE region, the South Pacific around 60 °S, and the subtropical eastern Pacific.

Corroborating with the reduced variance, the power spectrum peak of the PDV at about 14-17 years in the historical scenarios (Fig. 3d) is reduced by 20.5% and shifts to a marginal peak of 12-13 years in the SSP5-8.5 runs (Fig. 3g). The spectral bands of the northern and southern parts of PDV are around 14-18 and 14-16 years under the historical conditions (Fig. 3e and f), but their spectral energies are decreased by 23.2% and 30.7% under the SSP5-8.5 forcing, respectively (Fig. 3h and i). Both the northern and southern parts of PDV shift toward a higher frequency (about 12-14 and 11-12 years) in the SSP5-8.5. This power spectral change can be detected in most models.

Recent studies found a significant increase in global ocean heat content (OHC) since 1998, especially for the tropical and subtropical Pacific and southern Oceans with a robust OHC increase in the upper ocean (Cheng et al., 2017; Lyman et al., 2010; Liu et al., 2016). Meanwhile, both observations and models show that the ocean stratification is enhanced in global oceans, especially in the tropical Pacific (Fu et al., 2016; Yamaguchi & Suga, 2019). Under the SSP5-8.5 scenario (Fig. 4), anthropogenic warming also induces the stronger upper-ocean stratification and increased buoyancy frequency over the entire Pacific. The enhanced buoyancy frequency results in the faster westward-propagating Rossby waves (Fig. 4c and d), which is robust across most models (see Methods). The accelerated westward-propagating Rossby waves modulate the ocean gyre circulation and reduce the cross-basin time scale in both the North and South Pacific (Zhang & Delworth, 2016; Wang et al., 2007; Qiu & Chen, 2006). This plays a critical role in shortening the lifespan of the PDV (Fig. 3g-i) and limiting its growth time, which may reduce the PDV.

However, the decadal variability over the west coast of North America will not be increased under the anthropogenic warming (Fig. 3 and Fig. S3), which means that the enhanced variability over the west coast of North America and equatorial central Pacific for the D4-D3 (Fig. 1c and d) might not be related to global warming.

Observational data showed an increasing trend in the coupling between the positive PDO and negative NPGO in recent decades (Joh & Di Lorenzo, 2017). We checked the impact of NPGO on SST and atmospheric circulation with the NPGO index defined by Di Lorenzo et al. (2008). The result shows that the negative NPGO induces the warming over the west coast of North America and equatorial central Pacific and a north-south dipole SLP pattern over the northeast Pacific (Fig. S4), which resembles the SSTA and SLP anomaly patterns observed for the D4-D3 (Fig. 1 c and f). Furthermore, the composite positive PDO-negative NPGO events show much stronger warming over the west coast of North America and equatorial central Pacific than the positive PDO-positive NPGO events during both 1950-2019 and 1950-1998 (Fig. 5). During 1961-1998, the occurrence of positive PDO-negative NPGO events is 63% (27/43), while it is 81% (17/21) during 1999-2019. These results suggest that the coupling between the PDO and NPGO may play an important role in strengthening the decadal variability over the west coast of North America and equatorial central Pacific.

It is an open question for the dynamic mechanism of NPGO. Two popular mechanisms are proposed: one is the atmosphere stochastic forcing (Yi et al., 2015; Yi et al., 2018); the other is the central Pacific (CP) ENSO-induced atmospheric teleconnections (Di Lorenzo et al., 2010, 2013; Furtado et al., 2012), which favors a positive trend of NPGO/PDO correlation in future warming (Joh & Di Lorenzo, 2017). However, no matter which mechanism contributes to the current enhanced coupling between PDO and NPGO, the enhanced coupling would not be able to offset the weakened decadal variability over the west coast of North America under the anthropogenic warming based on both the CMIP5 and CMIP6 MME mean results (Fig. 3 and Fig. S3).

5 Concluding remarks

This study uses observational and reanalysis data to show that the recent PDV has distinctive characteristics and climate impacts. We also use CMIP6 modeling results to discuss the impact of anthropogenic forcing on the PDV change. The analyses suggest that the recent PDV pattern occurs mainly over the North Pacific with enhanced decadal variability over the west coast of North America and central Pacific, whereas reduced decadal variability in the KOE region. The magnitude of decadal variability in the South Pacific is much weaker, especially for the western South Pacific, the South Pacific cold tongue, the west coast of South America, and the southern Pacific Ocean along 60°S. The change in PDV also shows remarkably different impacts on land precipitation over northern North America and Greenland, Siberia, western Europe, tropical Africa, northeastern South America, and Northern Australia. The change means that the prediction of decadal variations of land precipitation based on the 20th century's PDV teleconnection is not applicable now.

The PDV change can be induced by the combination of anthropogenic warming and internal climate variability. Observational data shows that an increased coupling between the PDO and NPGO can contribute to the recent increased decadal variability over the west coast of North America and equatorial central Pacific. However, this decadal variability will not be enhanced under anthropogenic warming. CMIP6 MME mean results suggest that anthropogenic warming plays an important role in decreasing the SST decadal variability over the KOE region and South Pacific and shortening the PDV's periodicity. This is because global warming enhances the oceanic stratification that increases the speed of oceanic Rossby waves.

Our findings promote a deeper understanding of the recent PDV change along with the remarkably different impacts on global atmospheric circulation and precipitation and shed light on its future change under the increasing anthropogenic forcing. The result can be useful for infrastructure planning, disaster mitigation, food security, and water resource management in the coming decades.

Acknowledgments

We thank the ECMWF, GPCC, ERSST, HadISST, and CMIP5/6 for providing the data set. This research is jointly supported by the National Key Research and Development Program of China (2016YFA0600401), National Natural Science Foundation of China (41971108, 41420104002, 41671197, and 41971021), Program of Innovative Research Team of Jiangsu Higher Education Institutions of China, and Priority Academic Program Development of Jiangsu Higher Education Institutions (164320H116).

Data Availability

Data used in this paper can be downloaded from the following:

ERA-40 and ERA-5: https://www.ecmwf.int/en/forecasts/datasets/reanalysis-datasets/era5

HadISST: https://www.metoffice.gov.uk/hadobs/hadisst

ERSST: https://www.ncdc.noaa.gov/data-access/marineocean-data/extended-reconstructed-sea-surface-temperature-ersst-v5

GPCC: https://psl.noaa.gov/data/gridded/data.gpcc.html

CMIP6 data: https://esgf-node.llnl.gov/search/cmip6

CMIP5 data: https://pcmdi9.llnl.gov/projects/cmip5

References

Chelton, D. B., deSzoeke, R. A., Schlax, M. G., Naggar, K. E., & Siwertz, N. (1998) Geographical variability of the first baroclinic Rossby radius of deformation. *Journal of Physical Oceanography*, *28*, 433 – 460. https://doi.org/10.1175/1520-0485(1998)028<0433:GVOTFB>2.0.CO;2

Chen, X., & Wallace, J. M. (2015) ENSO-like variability: 1900-2013. *Journal of Climate*, *28*, 9623–9641. https://doi.org/10.1175/JCLI-D-15-0322.1

Cheng, L., Trenberth, K. E., Fasullo, J., Boyer, T., Abraham, J., & Zhu, J. (2017) Improved estimates of ocean heat content from 1960 to 2015. *Science Advances*, *3*, e1601545. https://doi.org/ 10.1126/sciadv.1601545

Dai, A. (2013) The influence of the inter-decadal Pacific oscillation on US precipitation during 1923-2010. *Climate Dynamics*, *41*, 633–646. https://doi.org/10.1007/s00382-012-1446-5

Di Lorenzo, E., Schneider, N., Cobb, K. M., Franks, P. J. S., Chhak, K., Miller, A. J., et al. (2008) North Pacific Gyre Oscillation links ocean climate and ecosystem change. *Geophysical Research Letters*, *35*, L08607. https://doi.org/10.1029/2007GL032838

Di Lorenzo, E., Cobb, K. M., Furtado, J. C., Schneider, N., Anderson, B. T., Bracco, A., et al. (2010) Central Pacific El Nino and decadal climate change in the North Pacific Ocean. *Nature Geoscience*, *3*, 762–765. https://doi.org/10.1038/ngeo984

Di Lorenzo, E., Combes, V., Keister, J. E., Strub, P. T., Thomas, A. C., Franks, P. J .S., et al. (2013) Synthesis of Pacific Ocean climate and ecosystem dynamics. *Oceanography*, *26*, 68–81. https://doi.org/10.5670/oceanog.2013.76

Di Lorenzo, E., & Mantua, N. (2016) Multi-year persistence of the 2014/15 North Pacific marine heatwave. *Nature Climate Cha*nge, *6*, 1042–1047. https://doi.org/10.1038/nclimate3082

Eyring, V., Bony, S., Meehl, G. A., Senior, C. A., Stevens, B., Stouffer, R. J., et al. Overview of the Coupled Model Intercomparison Project Phase 6 (CMIP6) experimental design and organization. *Geoscientific Model Development*, *9*, 1937–1958. https://doi.org/10.5194/gmd-9-1937-2016

Fu, W., Randerson, J. T., & Moore, J. K. (2016) Climate change impacts on net primary production (NPP) and export production (EP) regulated by increasing stratification and phytoplankton community structure in the CMIP5 models. *Biogeosciences*, *13*, 5151–5170. https://doi.org/10.5194/bg-13-5151-2016

Furtado, J. C., Di Lorenzo, E., Anderson, B. T., & Schneider N. (2012) Linkages between the North Pacific Oscillation and central tropical Pacific SSTs at low frequencies. *Climate Dynamics*, *39*, 2833–2846. https://doi.org/10.1007/s00382-011-1245-4

Geng, T., Yang, Y., & Wu, L. (2019) On the mechanisms of Pacific decadal oscillation modulation in a warming climate. *Journal of Climate*, *32*, 1443–1459. https://doi.org/10.1175/JCLI-D-18-0337.1

Hartmann, D. L. (2015) Pacific sea surface temperature and the winter of 2014. *Geophysical Research Letters*, *42*, 1894–1902. https://doi.org/10.1002/2015GL063083

Hu, Z.-Z., Kumar, A., Jha, B., Zhu, J., & Huang, B. (2017) Persistence and predictions of the remarkable warm anomaly in the Northeastern Pacific Ocean during 2014-2016. *Journal of Climate*, *30*, 689–702. https://doi.org/10.1175/JCLI-D-16-0348.1

Hersbach, H. *et al*. Operational global reanalysis: progress, future directions and synergies with NWP *ECMWF ERA Rep Series* 2018; **N27**. Available on: https://www.ecmwf.int/node/18765.

Huang, B., Thorne, P. W., Banzon, V. F., Boyer, T., Chepurin, G., Lawrimore, J. H., et al. (2017) Extended Reconstructed Sea Surface Temperature, Version 5 (ERSSTv5): Upgrades, Validations, and Intercomparisons. *Journal of Climate*, *30*, 8179–8205. https://doi.org/10.1175/JCLI-D-16-0836.1

Hus, H.-H., & Chen, Y.-L. (2011) Decadal to bi-decadal rainfall variation in the western Pacific: A footprint of South Pacific decadal variability? *Geophysical Research Letters*, *38*, L03703. https://doi.org/10.1029/2010GL046278

Joh, Y., Di Lorenzo, E. (2017) Increasing coupling between NPGO and PDO leads to prolonged marine heatwaves in the Northeast Pacific. *Geophysical Research Letters*, *44*, 11663–11671. https://doi.org/10.1002/2017GL075930

Kwon, Y. O., & Deser, C. (2007) North Pacific decadal variability in the Community Climate System Model version 2. *Journal of Climate*, *20*, 2416–2433. https://doi.org/10.1175/JCLI4103.1

Li, S., Wu, L., Yang, Y., Geng, T., Cai, W., Gan, B., et al. (2020) The pacific Decadal Oscillation less predictable under greenhouse warming. *Nature Climate Change*, *10*, 30–34. https://doi.org/10.1038/s41558-019-0663-x

Liu, Z., & Di Lorenzo, E. (2018) Mechanisms and predictability of Pacific decadal variability. *Current Climate Change Reports*, *4*, 128–144. https://doi.org/10.1007/s40641-018-0090-5

Liguori, G., & Di Lorenzo, E. (2018) Meridional modes and increasing Pacific decadal variability under anthropogenic forcing. *Geophysical Research Letters*, *45*, 983–991. https://doi.org/10.1002/2017GL076548

Liu, W., Xie, S.-P., & Lu, J. (2016) Tracking ocean heat uptake during the surface warming hiatus. *Nature Communications*, *7*, 10926. https://doi.org/10.1038/ncomms10926

Liu, Z. (2012) Dynamics of interdecadal climate variability: a historical perspective. *Journal of Climate*, *25*, 1963–1995. https://doi.org/10.1175/2011JCLI3980.1

Lyman, J. M., Good, S. A., Gouretski, V. V., Ishii, M., Johnson, G. C., Palmer, M. D. et al. (2012) Robust warming of the global upper ocean. *Nature*, *465*, 334–337. https://doi.org/10.1038/nature09043

Lyon, B., Barnston, A. G., & DeWitt, D. G. (2014) Tropical pacific forcing of a 1998–1999 climate shift: observational analysis and climate model results for the boreal spring season. *Climate Dynamics*, *43*, 893–909. https://doi.org/10.1007/s00382-013-1891-9

Mantua, N. J., Hare, S. R., Zhang, Y., Wallace, J. M., & Francis, R. C. (1997) A Pacific interdecadal climate oscillation with impacts on salmon production. *Bulletin of the American Meteorological Society*, *78*, 1069–1079. https://doi.org/10.1175/1520-0477(1997)078<1069:APICOW>2.0.CO;2

Mo, K. C. (2000) Relationships between low-frequency variability in the southern hemisphere and sea surface temperature anomalies. *Journal of Climate*, *13*, 3599–3610. https://doi.org/10.1175/1520-0442(2000)013<3599:RBLFVI>2.0.CO;2

Newman, M., Alexander, M. A., Ault, T. R., Cobb, K. M., Deser, C., Di Lorenzo, E., et al. (2016) The Pacific Decadal Oscillation, Revisited. *Journal of Climate*, *29*, 4399–4427. https://doi.org/10.1175/JCLI-D-15-0508.1

Power, S., Casey, T., Folland, C., Colman, A., & V. Mehta (1999) Inter-decadal modulation of the impact of ENSO on Australia. *Climate Dynamics*, *15*, 319–324. https://doi.org/10.1007/s003820050284

Qin, M., Li, D., Dai, A., Hua, W., & Ma, H. (2018) The influence of the Pacific Decadal Oscillation on North Central China precipitation during boreal autumn. *International Journal of Climatology*, *38*, 821–831. https://doi.org/10.1002/joc.5410

Qiu, B., & Chen, S. (2006) Decadal variability in the large-scale sea surface height field of the South Pacific Ocean: observations and causes. *Journal of Physical Oceanography*, *36*, 1751–1762. https://doi.org/10.1175/JPO2943.1

Rayner, N. A., Parker, D. E., Horton, E. B., Folland, C. K., Alexander, L. V., Rowell, D. P., et al. (2003) Global analyses of sea surface temperature, sea ice, and night marine air temperature since the late nineteenth century. *Journal of Geophysical Research: Atmospheres*, *108*, 447. https://doi.org/10.1029/2002JD002670

Schneider, N., Miller, A.J., & Pierce, D. W. (2002) Anatomy of North Pacific decadal variability. *Journal of Climate*, *15*, 586–605. https://doi.org/10.1175/1520-0442(2002)015<0586:AONPDV>2.0.CO;2

Schneider, U., Becker, A., Finger, P., Meyer-Christoffer, A., Ziese, M., & Rudolf, B. (2014) GPCC's new land surface precipitation climatology based on quality-controlled in situ data and its role in quantifying the global water cycle. *Theoretical and Applied Climatology*, *115*, 15–40. https://doi.org/10.1007/s00704-013-0860-x

Seager, R., Hoerling, M., Schubert, S., Wang, H., Lyon, B., Kumar, A., et al. (2015) Causes of the 2011-14 California Drought. *Journal of Climate*, *28*, 6997–7024. https://doi.org/10.1175/JCLI-D-14-00860.1

Taylor, K. E., Stouffer, R. J., & Meehl, G. A. (2012) An overview of CMIP5 and the experiment design. *Bulletin of the American Meteorological Society*, *93*, 485–498. https://doi.org/10.1175/BAMS-D-11-00094.1

Uppala, S. M., KÅllberg, P. W., Simmons, A. J., Andrae, U., Da Costa Bechtold, V., Fiorino, M. et al. (2005) The ERA-40 re-analysis. *Quarterly Journal of the Royal Meteorological Society*, *131*, 2961-3012. https://doi.org/10.1256/qj.04.176

Van Oldenborgh, G. J., Doblas-Reyes, F. J., Wouters, B., & Hazeleger, W. (2012) Decadal prediction skill in a multi-model ensemble. *Climate Dynamics*, *38*, 1263–1280. https://doi.org/10.1007/s00382-012-1313-4

Wang, S.-Y. S., Huang, W., & Yoon, J. H. (2015) The North American winter `dipole' and extremes activity: a CMIP5 assessment. *Atmospheric Science Letters*, *16*, 338–345. https://doi.org/10.1002/asl2.565

Wang, X., Li, C., & Zhou, W. (2007) Interdecadal mode and its propagating characteristics of SSTA in the South Pacific. *Meteorology and Atmospheric Physics*, *98*, 115–124. https://doi.org/10.1007/s00703-006-0235-2

Whitney, F. A. (2014) Anomalous winter winds decrease 2014 transition zone productivity in the NE Pacific. *Geophysical Research Letters*, *42*, 428–431. https://doi.org/10.1002/2014GL062634

Yamaguchi, R., & Suga, T. (2019) Trend and variability in global upper-ocean stratification since the 1960s. *Journal of Geophysical Research: Oceans*, *124*, 8933–8948. https://doi.org/10.1029/2019JC015439

Yi, D., Zhang, L., & Wu, L. (2015) On the mechanisms of decadal variability of the North Pacific Gyre Oscillation over the 20th century. *Journal of Geophysical Research: Oceans*, *120*, 6114–6129. https://doi.org/10.1002/2014JC010660

Yi, D., Gan, B., Wu, L., & Miller, A. J. (2018) The North Pacific Gyre Oscillation and Mechanisms of its Decadal Variability in CMIP5 Models. *Journal of Climate*, *31*, 2487–2509. https://doi.org/10.1175/JCLI-D-17-0344.1

Zhang, L. P., & Delworth, T. L. (2016) Simulated response of the Pacific decadal oscillation to climatic change. *Journal of Climate*, *29*, 5999–6018. https://doi.org/10.1175/JCLI-D-15-0690.1

Zhang, Y., Xie, S.-P., Kosaka, Y., & Yang, J.-C. (2018) Pacific decadal oscillation: Tropical Pacific forcing versus internal variability. *Journal of Climate*, *31*, 8265–8279. https://doi.org/10.1175/JCLI-D-18-0164.1

Figure captions

Figure 1. Observed change in the PDV mode. (a) The time series of 30-month running mean PDV index. Blue shadings represent the period 1961-1976 (D1) and 1999-2013 (D3), while red shadings represent the period 1977-1998 (D2) and 2014-2019 (D4). (b) and (c) represent the differences in detrended annual mean SST anomalies (℃) for D2 minus D1 and for D4 minus D3, respectively. (d) denotes the results in (c) minus (b). The contours in (d) denote the SST anomalies for D2 minus D1. (e–g) same as (b–d), but for sea level pressure (shading, hPa) and 10m winds (vectors, m s^{-1}). Only the anomalies with confidence level exceeding the 90% (via a two-tailed Student's *t* test) are displayed in (b), (c), (e), and (f).

Figure 2. Change in the PDV's impact on precipitation and atmospheric circulation. The differences in annual mean 850 hPa winds (m s^{-1}), land precipitation (shading over the land, mm/day), and SST (shading over the ocean, ℃) anomalies for D2 minus D1 (a) and D4 minus D3 (b), respectively. The arrows denote composite 850 hPa wind anomalies, which are hidden over the land region. (c) and (d) same as (a) and (b), but for the vertical velocity at 500 hPa (10^{-2} Pa s^{-1}). Only the anomalies with confidence level exceeding the 90% (via a two-tailed Student's *t* test) are displayed.

Figure 3. Simulated change in the pattern and periodicity of PDV under greenhouse warming. The multi-model ensemble mean of the EOF1 from 33 CMIP6 models under the historical (a) and SSP5-8.5 (b) conditions. (c) denotes the PDV pattern changes between the SSP5-8.5 and the Historical condition. Black horizontal line denotes the equator. (d–f) Power spectrum of SST PC1 of the PDV, North Pacific (0-70N), and South Pacific (0-70S), respectively, under the Historical condition. The dashed red line represents the 90% confidence level. (g–i) same as (d–f), but for the SSP5-8.5 scenario.

Figure 4. Simulated change in buoyancy frequency and Rossby wave speed. (a) The buoyancy frequency (10^{-3} s^{-1}) over the South Pacific region (10S-60S, 140E-70W) under the Historical (blue), SSP5-8.5 (red), and SSP5-8.5 minus historical (orange) conditions. (b) same as (a), but for over the North Pacific region (10N-60N, 120E-100W). (c) Change rate of the zonally averaged first-baroclinic Rossby wave speed (m s^{-1}) over the South Pacific region between the SSP5-8.5 and the Historical condition. The phase speed is negative over the Pacific, which denotes westward propagation. (d) same as (c), but for over the North Pacific region. Shading represents twice the standard deviation.

Figure 5. SST variation during different phases of PDO and NPGO. Composite SST anomalies during 1950-2019 for (a) positive PDO–negative NPGO events (+P-N) minus negative PDO–positive NPGO events (-P+N) and (b) positive PDO–positive NPGO events (+P+N) minus negative PDO–negative NPGO events (-P-N). (c) denotes the results in (a) minus (b). (d–f) same as (a–c), but for the results during 1950-1998.

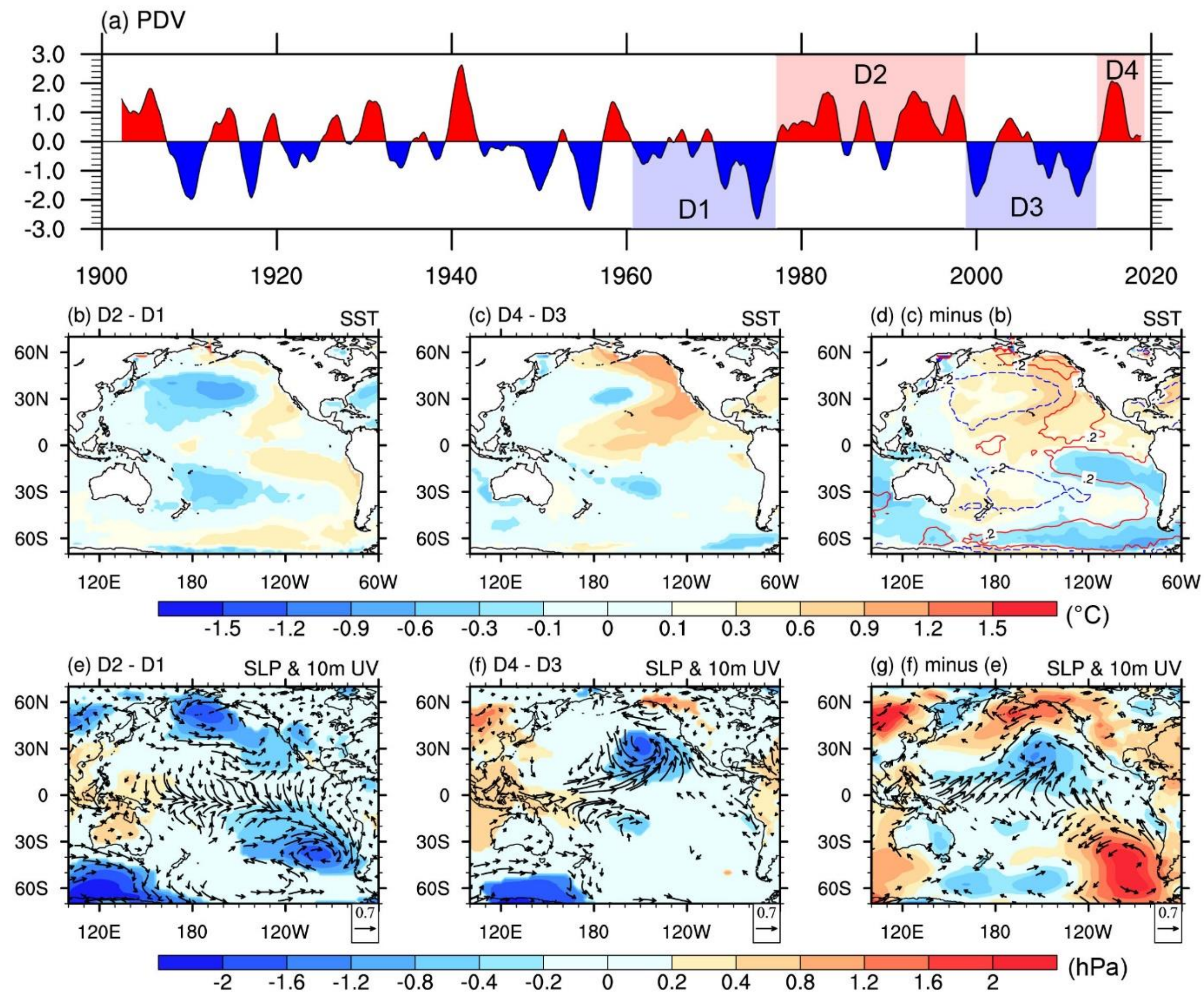

Figure 1. Observed change in the PDV mode. (a) The time series of 30-month running mean PDV index. Blue shadings represent the period 1961-1976 (D1) and 1999-2013 (D3), while red shadings represent the period 1977-1998 (D2) and 2014-2019 (D4). (b) and (c) represent the differences in detrended annual mean SST anomalies (℃) for D2 minus D1 and for D4 minus D3, respectively. (d) denotes the results in (c) minus (b). The contours in (d) denote the SST anomalies for D2 minus D1. (e–g) same as (b–d), but for sea level pressure (shading, hPa) and 10m winds (vectors, m s^{-1}). Only the anomalies with confidence level exceeding the 90% (via a two-tailed Student's *t* test) are displayed in (b), (c), (e), and (f).

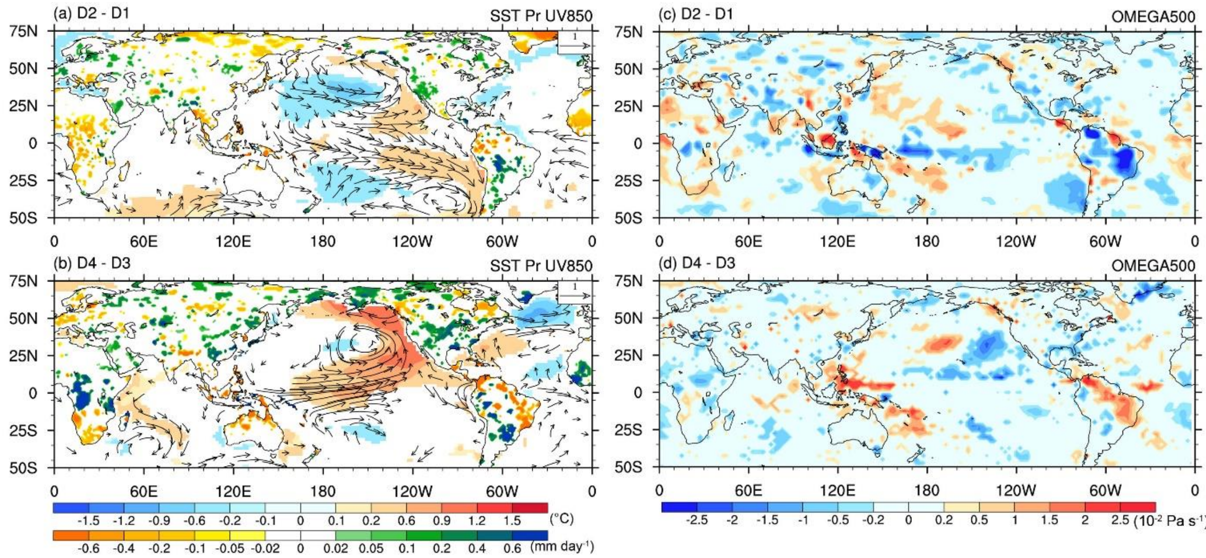

Figure 2. Change in the PDV's impact on precipitation and atmospheric circulation. The differences in annual mean 850 hPa winds (m s^{-1}), land precipitation (shading over the land, mm/day), and SST (shading over the ocean, ℃) anomalies for D2 minus D1 (a) and D4 minus D3 (b), respectively. The arrows denote composite 850 hPa wind anomalies, which are hidden over the land region. (c) and (d) same as (a) and (b), but for the vertical velocity at 500 hPa (10^{-2} Pa s^{-1}). Only the anomalies with confidence level exceeding the 90% (via a two-tailed Student's *t* test) are displayed.

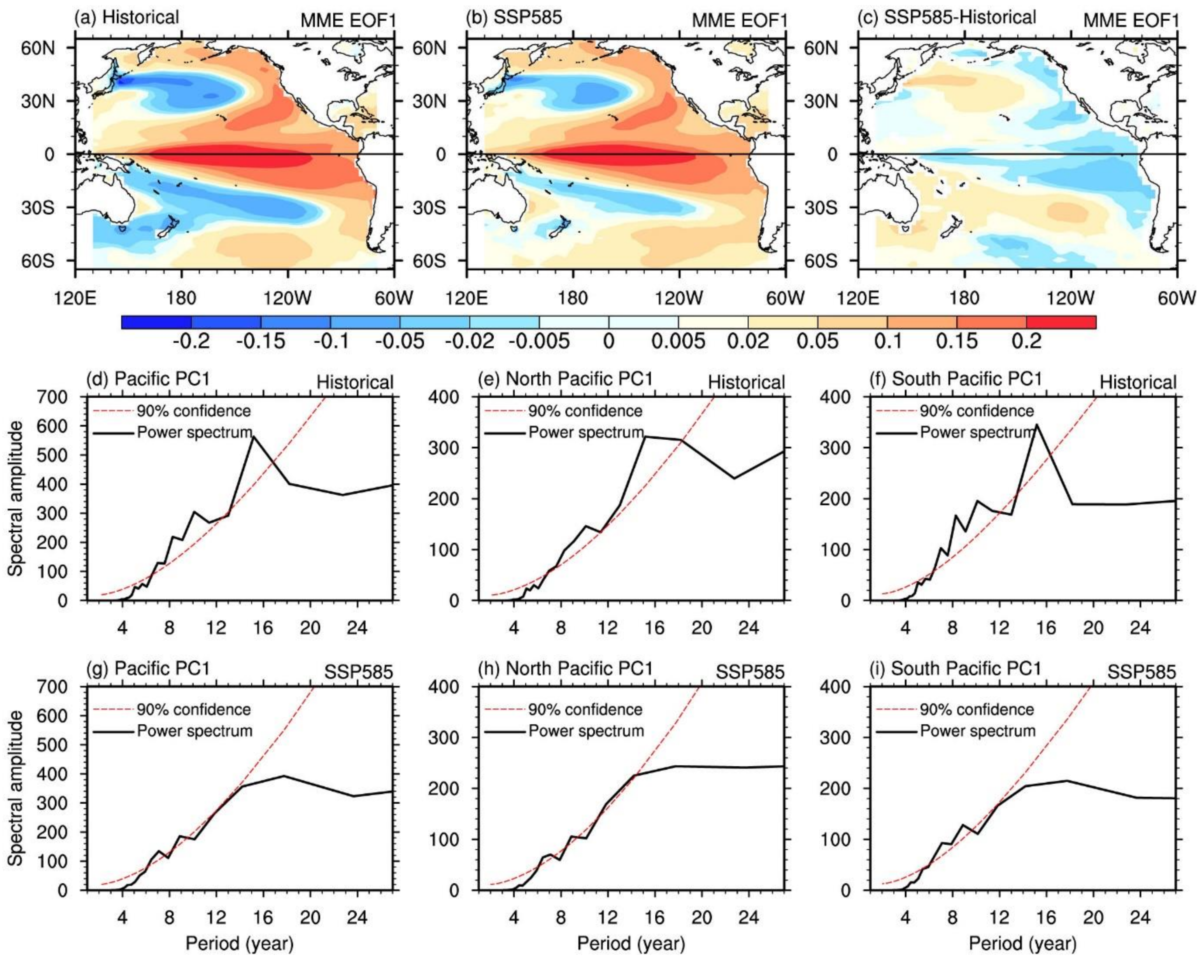

Figure 3. Simulated change in the pattern and periodicity of PDV under greenhouse warming. The multi-model ensemble mean of the EOF1 from 33 CMIP6 models under the historical (a) and SSP5-8.5 (b) conditions. (c) denotes the PDV pattern changes between the SSP5-8.5 and the Historical condition. Black horizontal line denotes the equator. (d–f) Power spectrum of SST PC1 of the PDV, North Pacific (0-70N), and South Pacific (0-70S), respectively, under the Historical condition. The dashed red line represents the 90% confidence level. (g–i) same as (d–f), but for the SSP5-8.5 scenario.

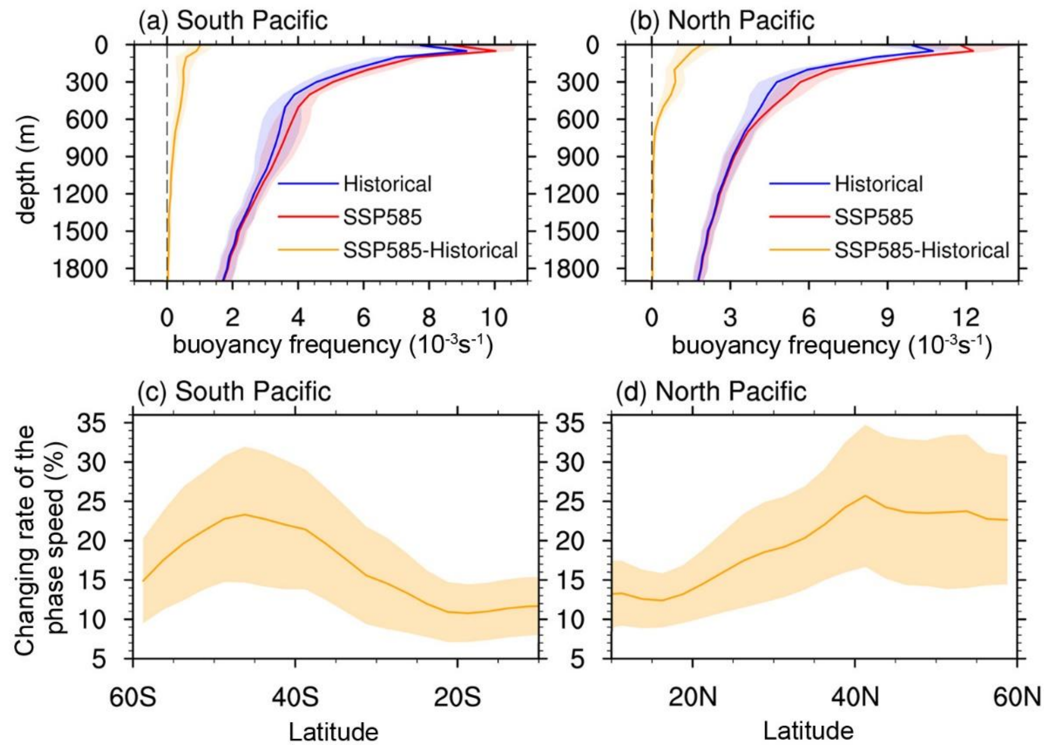

Figure 4. Simulated change in buoyancy frequency and Rossby wave speed. (a) The buoyancy frequency (10^{-3} s^{-1}) over the South Pacific region (10S-60S, 140E-70W) under the Historical (blue), SSP5-8.5 (red), and SSP5-8.5 minus historical (orange) conditions. (b) same as (a), but for over the North Pacific region (10N-60N, 120E-100W). (c) Change rate of the zonally averaged first-baroclinic Rossby wave speed (m s^{-1}) over the South Pacific region between the SSP5-8.5 and the Historical condition. The phase speed is negative over the Pacific, which denotes westward propagation. (d) same as (c), but for over the North Pacific region. Shading represents twice the standard deviation.

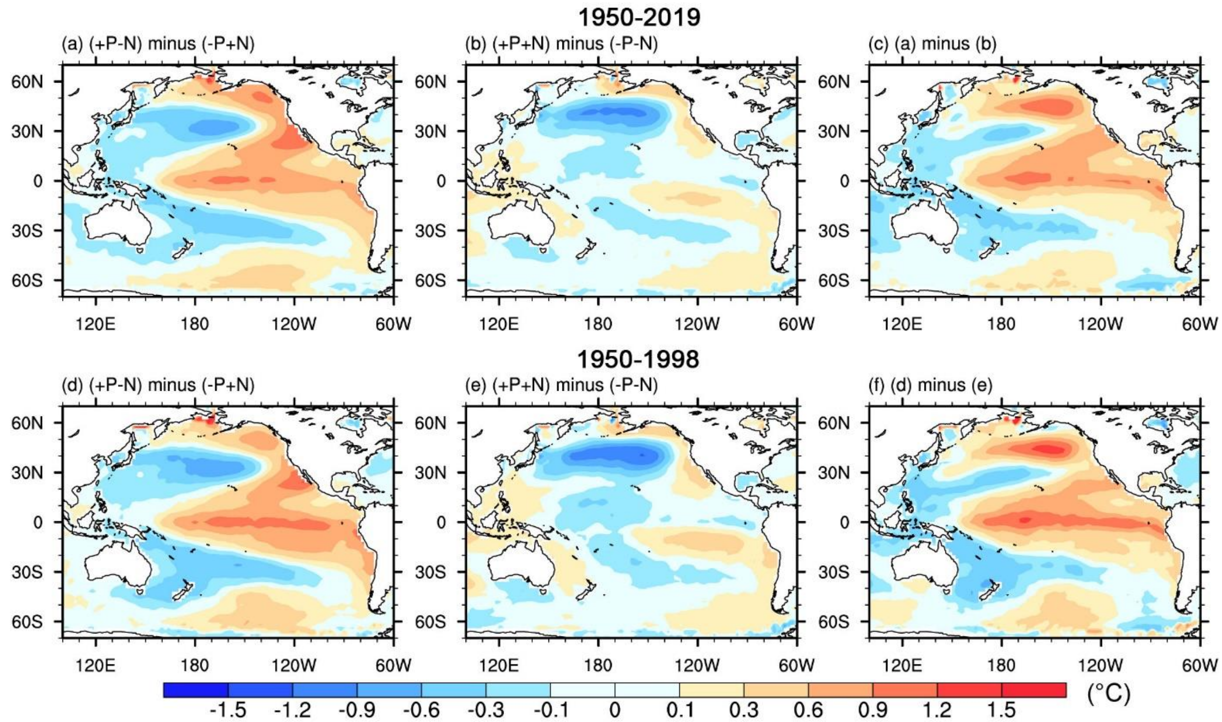

Figure 5. SST variation during different phases of PDO and NPGO. Composite SST anomalies during 1950-2019 for (a) positive PDO–negative NPGO events (+P-N) minus negative PDO–positive NPGO events (-P+N) and (b) positive PDO–positive NPGO events (+P+N) minus negative PDO–negative NPGO events (-P-N). (c) denotes the results in (a) minus (b). (d–f) same as (a–c), but for the results during 1950-1998.